Electronic Supplementary Information

Experimental section

Materials: Sodium fluride (NaF), ferric chloride hexahydrate ($FeCl_3 \cdot 6H_2O$), ammonium chloride (NH_4Cl), anhydrous lithium perchlorate ($LiClO_4$), hydrazine hydrate ($N_2H_4 \cdot H_2O$), sodium hypochlorite (NaClO), sodium hydroxide (NaOH), sodium salicylate ($C_7H_5O_3Na$), ethanol (CH_3CH_2OH), and carbon paper were bought from Beijing Chemical Corporation. Para-(dimethylamino) benzaldehyde ($C_9H_{11}NO$), sodium nitroferricyanide (III) dihydrate ($Na_2Fe(CN)_5NO \cdot 2H_2O$), and Nafion were purchased from Aladdin Ltd. (Shanghai, China). The water used throughout all experiments was purified through a Millipore system.

Preparation of β-FeO(OH,F): In the synthesis of typical sample, 8.0 mmol NaF and 16.0 mmol $FeCl_3 \cdot 6H_2O$ were dissolved in a mixture of 35 mL H_2O and 35 mL ethanol at room temperature. In what follows, the value of R_F with 0, 0.1, 0.3, 0.5, and 0.7, is used to describe the molar ratio of NaF to $FeCl_3 \cdot 6H_2O$. After continuously stirring for 30 min, the solution was transferred to 100 mL of Teflon-lined stainless autoclave. The autoclave was sealed and heated at 120 °C and kept at that temperature for 5 h. The product was washed with deionized water and ethanol for several times, dried in vacuum at 60 °C for 3 h to obtain the β-FeO(OH,F) nanorod.

Preparation of β-FeO(OH,F)/CP: Carbon paper (CP) was cleaned via brief sonication with ethanol and water for several times. To prepare the β-FeO(OH,F)/CP, 10 mg β-FeO(OH,F) and 40 μL 5 wt% Nafion solution were dispersed in 960 μL water/ethanol (V : V = 1 : 3) followed by 1-h sonication to form a homogeneous ink. 20 μL ink was loaded onto a CP (1 × 1 cm^2) and dried under ambient condition. The β-FeO(OH,F)/CP working electrode was prepared well.

Characterizations: TEM images were collected on a HITACHI H-8100 electron microscopy (Hitachi, Tokyo, Japan) operated at 200 kV. XPS measurements were performed on an ESCALABMK II X-ray photoelectron spectrometer using Mg as the exciting source. Raman spectra were obtained by a Renishaw inVia confocal Raman microprobe under 532 nm laser excitation. ICP-MS analysis was performed on ThermoScientific iCAP6300. The absorbance data of spectrophotometer were acquired on SHIMADZU UV-1800 UV-Vis spectrophotometer. A gas chromatograph (SHIMADZU, GC-2014C) equipped with MolSieve 5A column and Ar carrier gas

was used for H_2 quantifications. Gas-phase product was sampled every 1000 s using a gas-tight syringe (Hamilton). ^{1}H nuclear magnetic resonance (NMR) spectra were collected on a superconducting-magnet NMR spectrometer (Bruker AVANCE III HD 500 MHz) and dimethyl sulphoxide was used as an internal to calibrate the chemical shifts in the spectra.

Electrochemical measurements: Electrochemical NRR measurements were performed in a two-compartment cell separated by Nafion membrane using a CHI 660E electrochemical analyzer (CH Instruments, Inc., Shanghai) using a standard three-electrode system using β-FeO(OH,F)/CP as the working electrode, graphite plate as the counter electrode and Ag/AgCl as the reference electrode. The potentials reported in this work were converted to RHE scale via calibration with the following equation: E (vs. RHE) = E (vs. Ag/AgCl) + 0.059 × pH + 0.197 V and the presented current density was normalized to the geometric surface area. For electrochemical N_2 reduction, chrono-amperometry tests were conducted in N_2-saturated 0.5 M $LiClO_4$ solution (the $LiClO_4$ electrolyte was purged with N_2 for 30 min before the measurement).

Determination of NH_3: Concentration of produced NH_3 was spectrophotometrically determined by the indophenol blue method.[1] In detail, 4 mL electrolyte was obatined from the cathodic chamber and mixed with 50 μL oxidizing solution containing NaClO (ρCl = 4 ~ 4.9) and NaOH (0.75 M), 500 μL coloring solution containing 0.4 M $C_7H_6O_3Na$ and 0.32 M NaOH, and 50 μL catalyst solution (1 wt% $Na_2[Fe(CN)_5NO]$) for 1 h. Absorbance measurements were performed at λ = 655 nm. The concentration-absorbance curve was calibrated using standard NH_4^+ solution with a series of concentrations. The fitting curve ($y = 0.363x + 0.013$, $R^2 = 0.999$) shows good linear relation of absorbance value with NH_4^+ concentration.

Determination of N_2H_4: The N_2H_4 possibly was estimated by the method of Watt and Chrisp.[2] A mixed solution of 5.99 g $C_9H_{11}NO$, 30 mL concentrated HCl and 300 ml ethanol was used as a color reagent. Calibration curve was plotted as follow: firstly, preparing a series of N_2H_4 solutions of known concentration as standards; secondly, adding 5 mL color reagent to above N_2H_4 solution, separately, and standing 20 min at room temperature; finally, the absorbance of the resulting solution was measured at 460 nm. The fitting curve shows good linear relation of absorbance with $N_2H_4 \cdot H_2O$

concentration (y = 0.595x + 0.034, R^2 = 0.999) by three times independent calibrations.

Determination of FE and V_{NH3}: NH_3 formation rate was calculated using the following equation:

$$NH_3 \text{ yields} = [NH_4^+] \times V/(m_{cat.} \times t)$$

FE was calculated according to following equation:

$$FE = 3 \times F \times [NH_4^+] \times V/(18 \times Q)$$

Where $[NH_4^+]$ is the measured NH_4^+ concentration; V is the volume of the cathodic reaction electrolyte; t is the potential applied time; $m_{cat.}$ is the loaded quality of catalyst; F is the Faraday constant; and Q is the quantity of charge in Coulombs.

Computational details: First-principles density functional theory (DFT) calculations were performed with the generalized gradient approximation (GGA)[3] in the form of the Perdew, Burke, and Ernzerhof (PBE)[4] exchange-correlation functional, as implemented in the Dmol[3] package.[5] A six atom layers β-FeOOH surface was modeled for F-substitution with 20 Å vacuum space to avoid the interaction form nearby layers. Layers 1 to 3 are surface layers, and layers 4 to 6 are central layers. Both one OH group from surface and internal of β-FeOOH was replaced by F atom, named as β-FeO(OH,sF) and β-FeO(OH,iF), respectively. Structural relaxation was performed until the convergence criteria for energy were set to be 10^{-5} eV, and 0.002 Ha $Å^{-1}$ was adopted for the total energy calculations. The N_2 dissociation minimum energy path (MEP) was obtained by LST/QST tools in DMol[3] code.[6] The Brillouin zone integration was performed with 1 × 4 × 1 Γ-centred Monkhorst-Pack k-point meshes in geometry optimization. Frequencies of each complex were calculated after geometry optimization, and the free energy was obtained as follows:

$$\triangle G = \triangle E + \triangle ZPE - T\triangle S + \triangle G_u + \triangle G_{pH}$$

where △E, △ZPE and △S represent the difference in DFT-calculated total energy change, zero-point energy and the change in entropy between the products and reactants, respectively. T represents the temperature (298.15 K). $\triangle G_U = -neU$, where *n* represents the number of transferred charge, and U represents the electrode potential with respect to the normal hydrogen electrode. $\triangle G_{pH}$ represents the correction H^+ free energy by the concentration, which can be calculated through $\triangle G_{pH} = 0.059 \times pH$

(the value of pH is assumed to be zero in this work). The N_2 adsorption energy is defined as: $E_{ads} = E_{N2/substrate} - E_{substrate} - E_{N2}$.

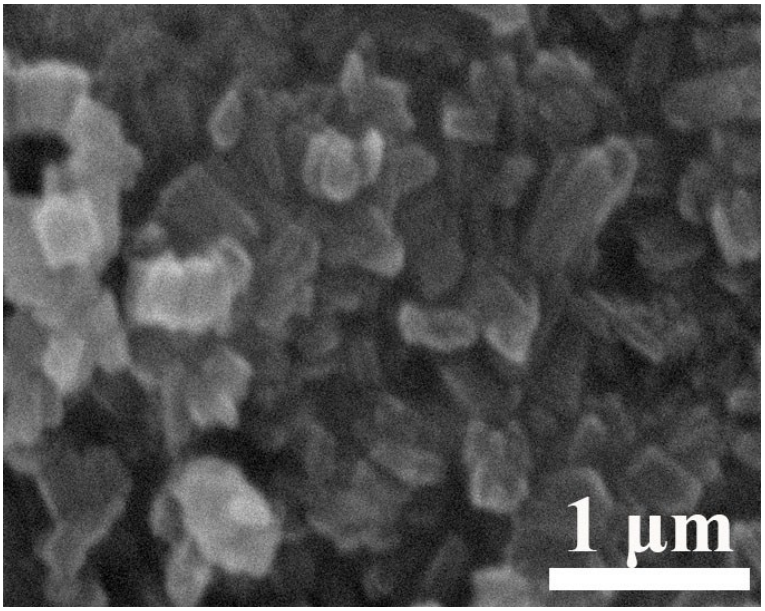

Fig. S1. SEM image of β-FeO(OH,F).

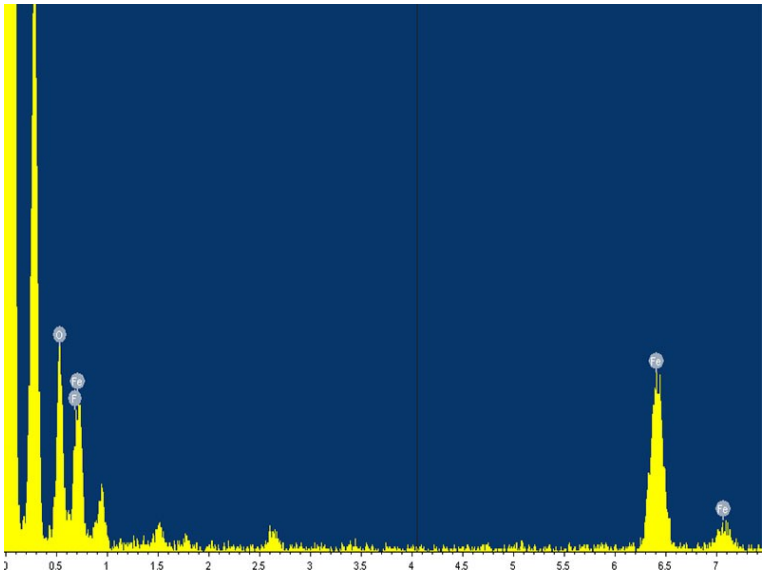

Fig. S2. EDX spectrum of β-FeO(OH,F).

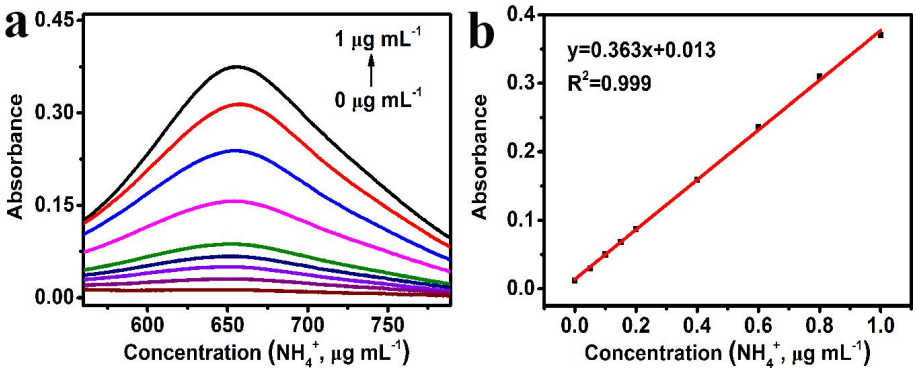

Fig. S3. (a) UV-Vis absorption spectra of indophenol assays with NH_4^+ concentrations after incubated for 1 h at room temperature. (b) Calibration curve used for calculation of NH_4^+ concentrations.

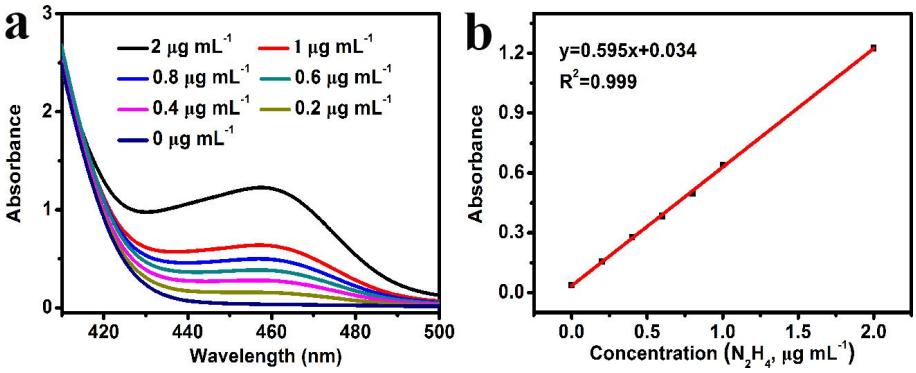

Fig. S4. (a) UV-Vis absorption spectra of N_2H_4 concentrations after incubated for 20 min at room temperature. (b) Calibration curve used for calculation of N_2H_4 concentrations.

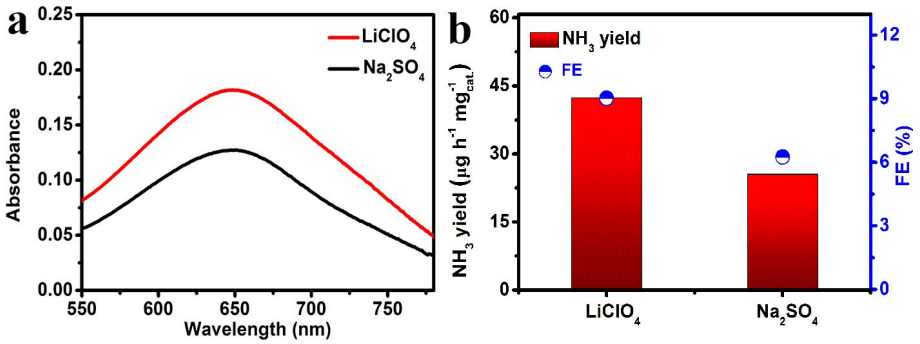

Fig. S5. (a) UV-Vis absorption spectra of different electrolyte stained with indophenol indicator after charging at –0.60 V. (b) NH_3 yields and FEs for β-FeO(OH,F) at –0.60 V in 0.1 M Na_2SO_4 and 0.5 M $LiClO_4$.

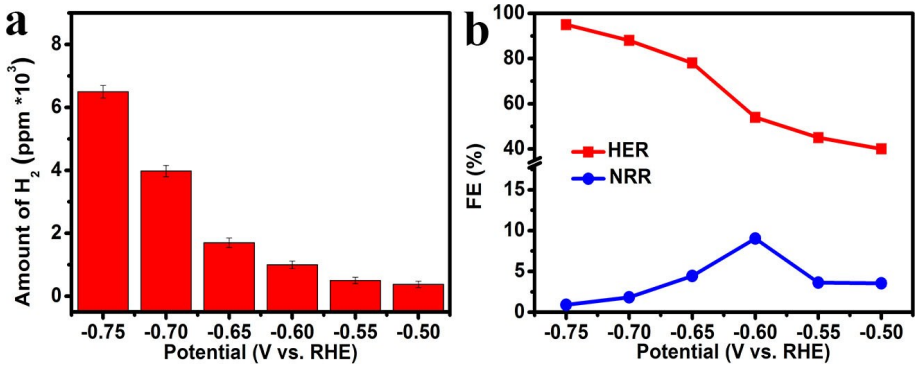

Fig. S6. (a) Amounts of H_2 from gas chromatography (GC) data of the gas from the headspace of the cell for NRR on the β-FeO(OH,F) in N_2-saturated 0.5 M $LiClO_4$ at various potentials. (b) The calculated FEs of HER and NRR.

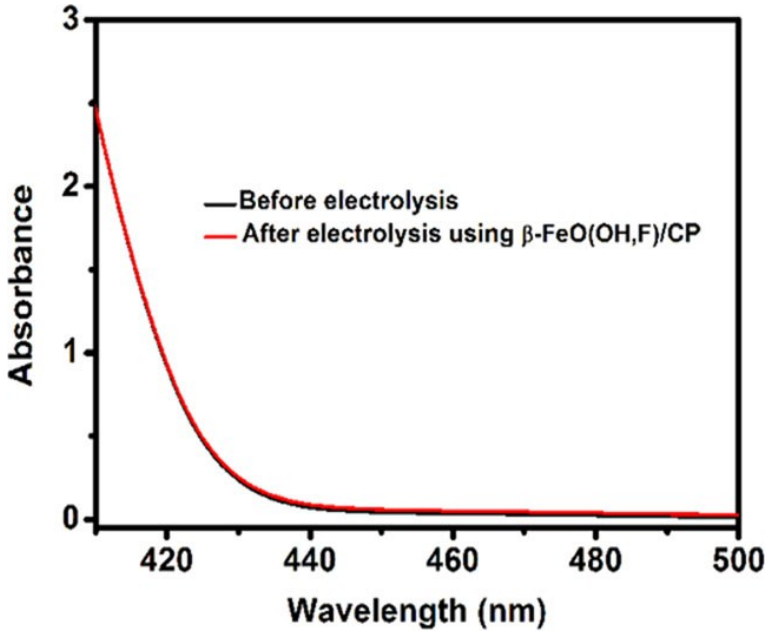

Fig. S7. UV-Vis absorption spectra of electrolytes stained with para-(dimethylamino) benzaldehyde indicator before and after 2 h electrolysis.

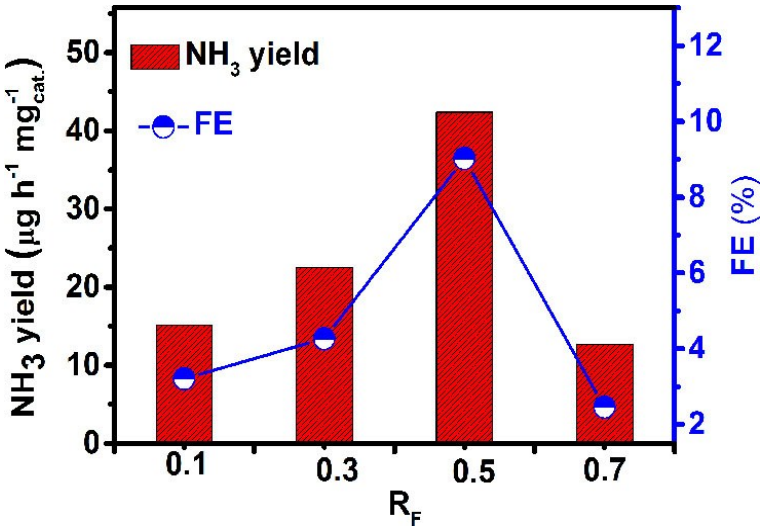

Fig. S8. NH_3 yields and FEs of β-FeO(OH,F) with various R_F values at −0.60 V.

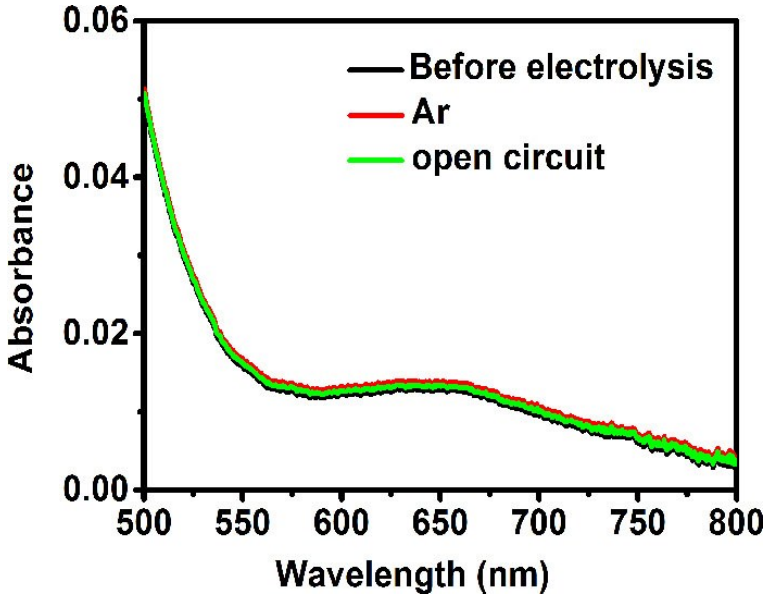

Fig. S9. UV-Vis absorption spectra of the electrolyte stained with indophenol indicator after charging at –0.60 V for 2 h under different electrochemical conditions.

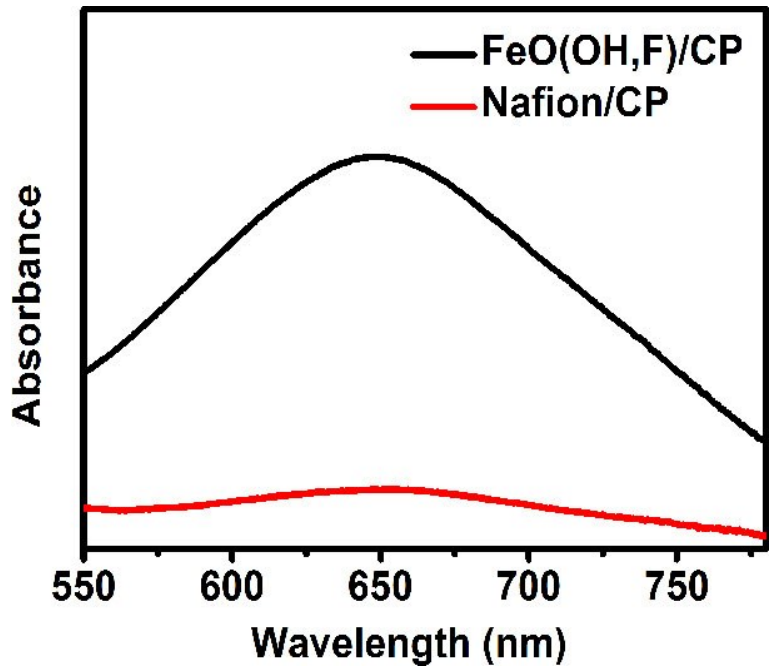

Fig. S10. UV-Vis absorption spectra of the electrolyte stained with indophenol indicator after charging at –0.60 V for 2 h using Nafion dispersed carbon paper.

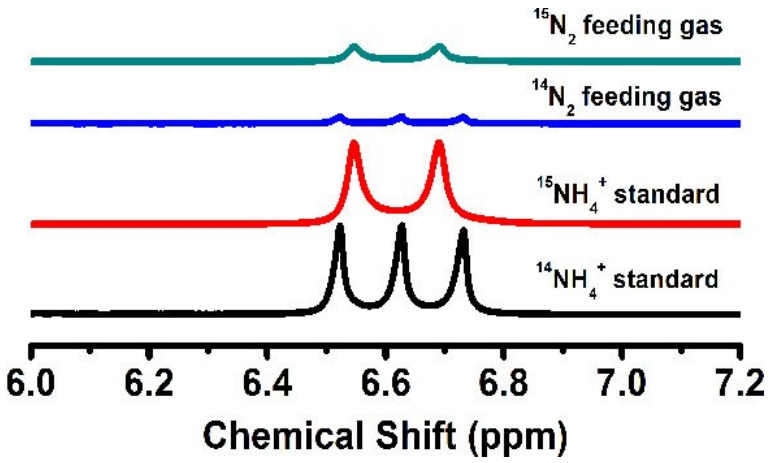

Fig. S11. ^{15}N isotope labeling experiment. ^{1}H NMR spectra for the post-electrolysis 0.5 M $LiClO_4$ electrolytes with $^{15}N_2$, $^{14}N_2$ as the feeding gas. Also shown are the spectra for $^{15}NH_4^+$ and $^{14}NH_4^+$ standard samples.

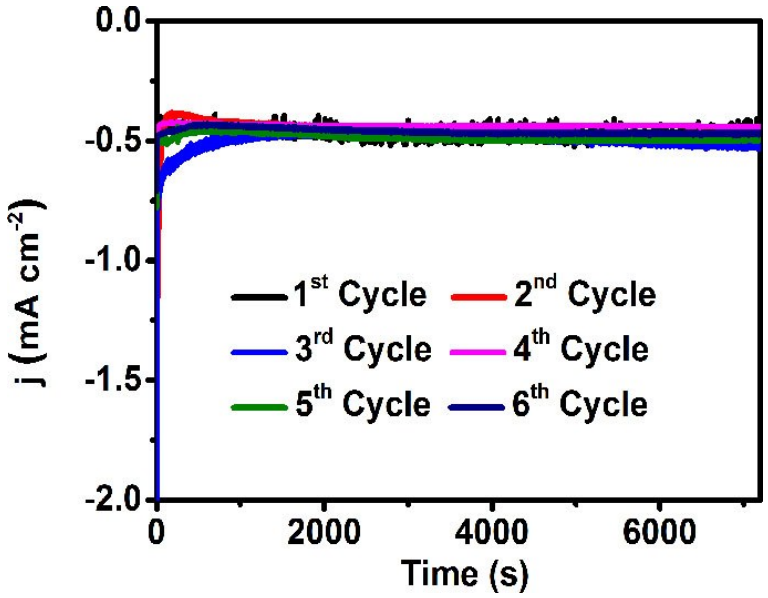

Fig. S12. Time-dependent current density curves of β-FeO(OH,F)/CP at –0.60 V for 6 consecutive cycles.

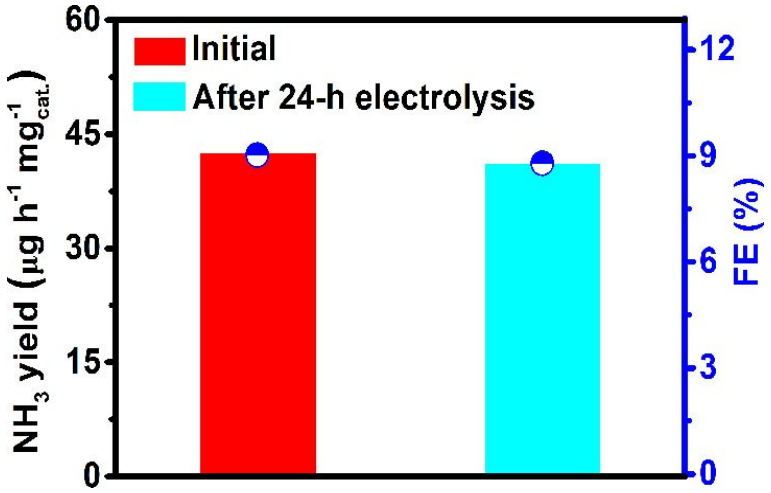

Fig. S13. NH_3 yields and FEs after charging at –0.60 V for 2 and 24 h.

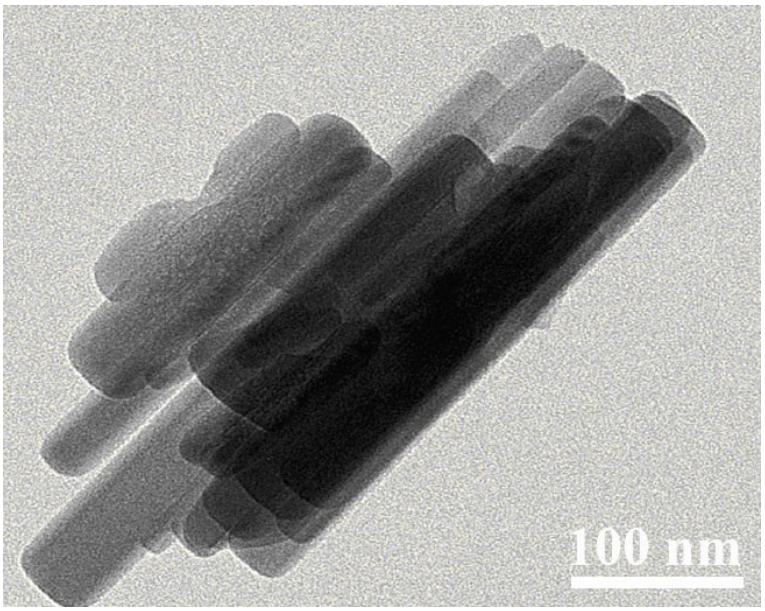

Fig. S14. TEM image of β-FeO(OH,F) after stability test.

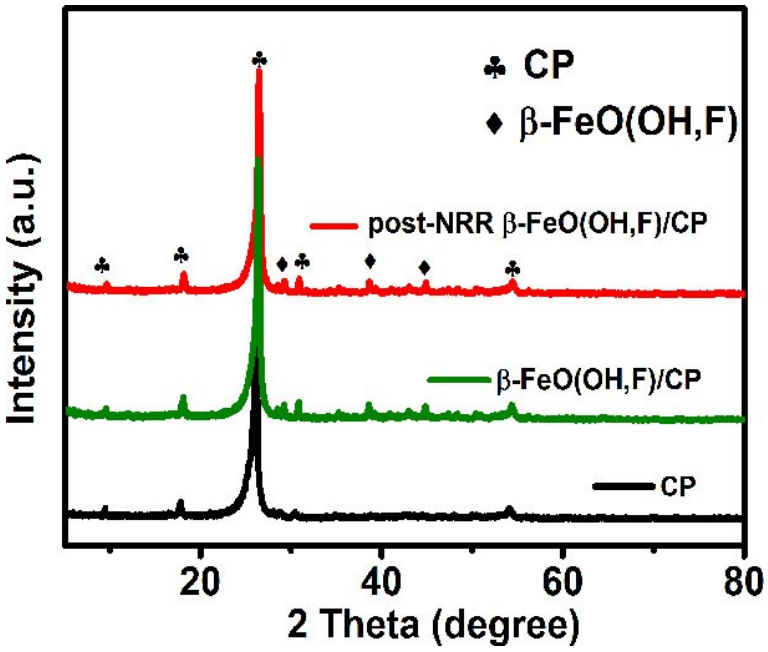

Fig. S15. XRD patterns of bare CP, β-FeO(OH,F)/CP, and post-NRR β-FeO(OH,F)/CP.

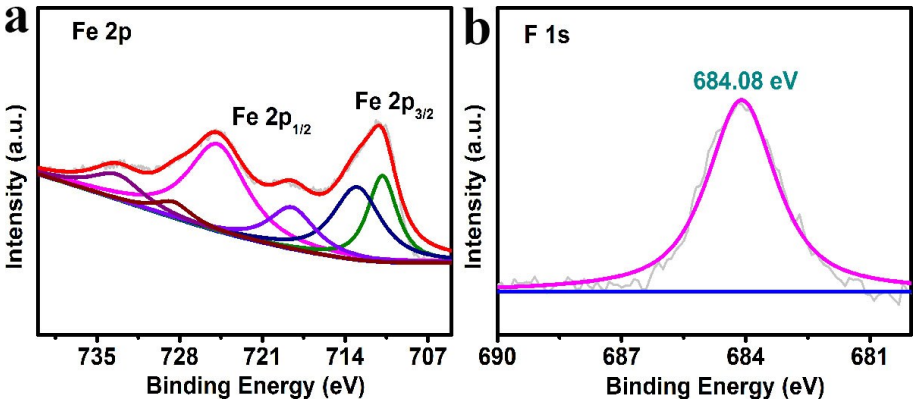

Fig. S16. XPS spectra of post-NRR β-FeO(OH,F) in (a) Fe 2p and (b) F 1s regions.

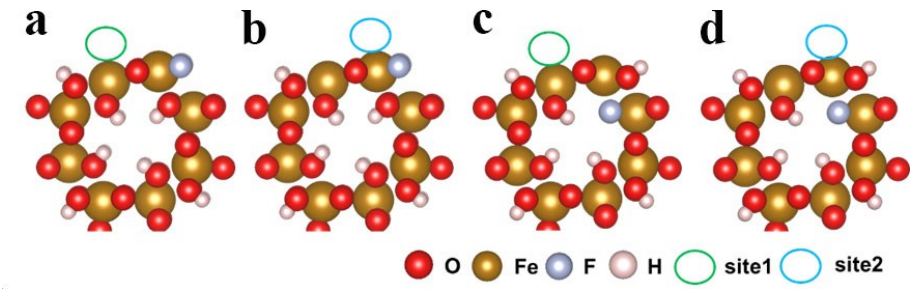

Fig. S17. Structures of (a) β-FeO(OH,sF-1), (b) β-FeO(OH,sF-2), (c) β-FeO(OH,iF-1), and (d) β-FeO(OH,iF-2).

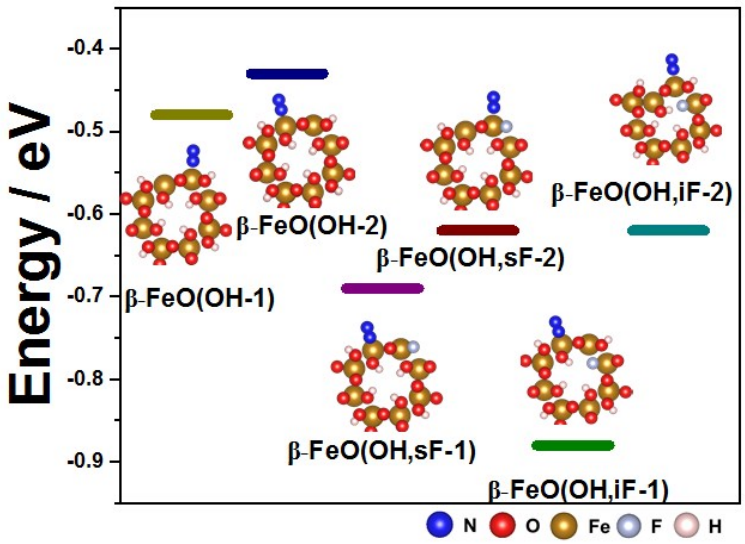

Fig. S18. Structures and calculated adsorption energies of N_2 adsorption on (200) surface of β-FeO(OH-1), β-FeO(OH-2), β-FeO(OH,sF-1), β-FeO(OH,sF-2), β-FeO(OH,iF-1), and β-FeO(OH,iF-2) for end-on configurations.

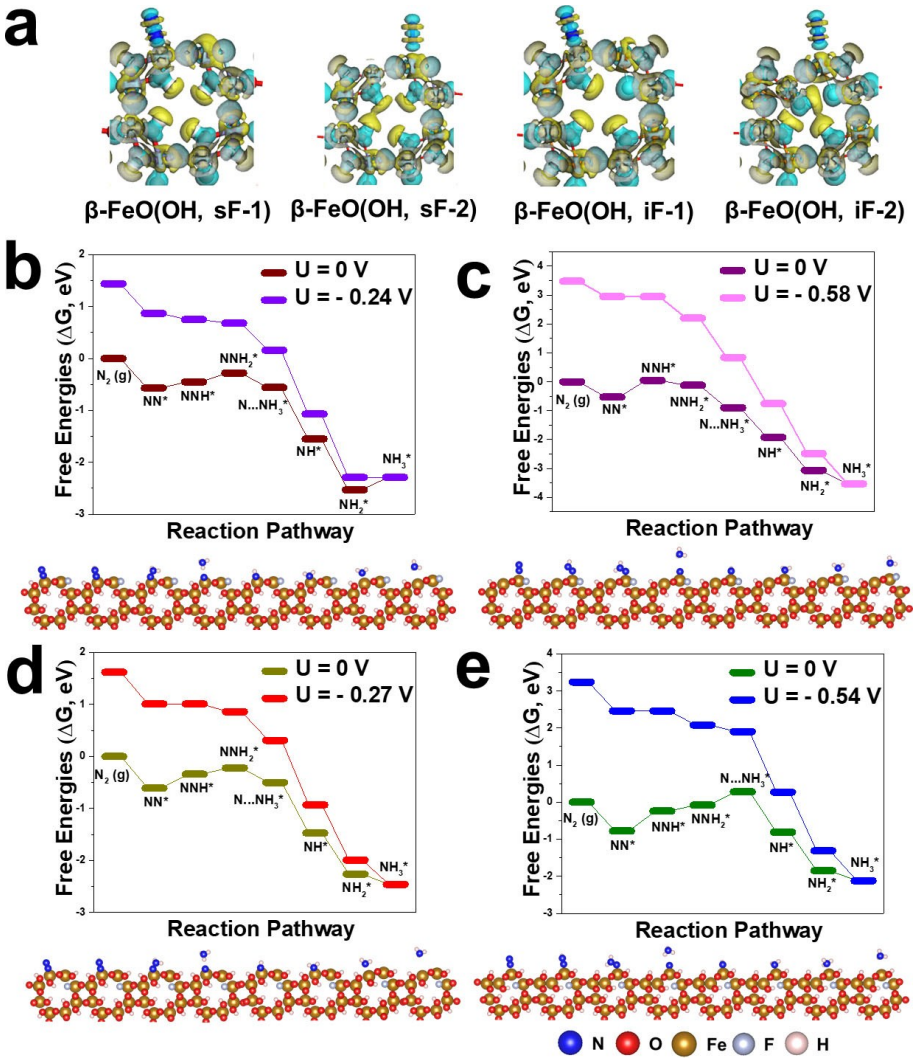

Fig. S19. (a) The optimized end-on configurations with the color-mapped charge density difference of N_2 adsorption on the (200) surface of β-FeO(OH,sF-1), β-FeO(OH,sF-2), β-FeO(OH,iF-1) and β-FeO(OH,iF-2). Yellow and cyan colors represent charge accumulation and charge depletion zones, respectively, with a isosurface value of 0.03 eV/Å^3. Free energy diagram and the optimized structures for the NRR at zero and applied potential (limiting potential) through distal mechanisms on (200) surface of (b) β-FeO(OH,sF-1), (c) β-FeO(OH,sF-2), (d) β-FeO(OH,iF-1), and (e) β-FeO(OH,iF-2).

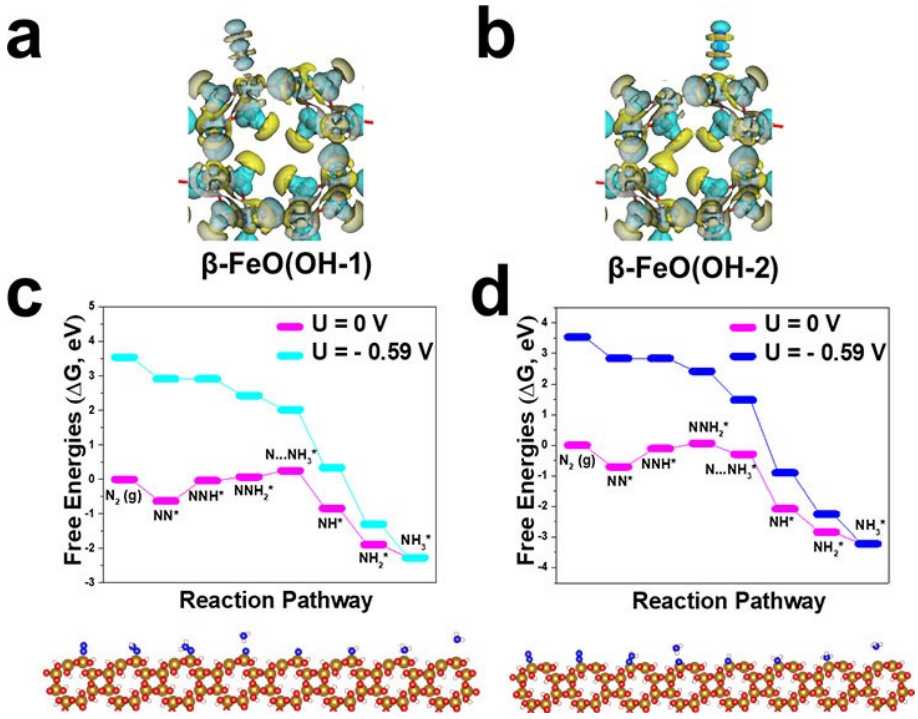

Fig. S20. The optimized end-on configurations with the color-mapped charge density difference of N_2 adsorption on the (200) surface of (a) β-FeO(OH-1) and (b) β-FeO(OH-2). Yellow and cyan colors represent charge accumulation and charge depletion zones, respectively, with a isosurface value of 0.03 eV/Å^3. Free energy diagram and the optimized structures for the NRR at zero and applied potential (limiting potential) through distal mechanisms on (200) surface of (c) β-FeO(OH-1) and (d) β-FeO(OH-2).

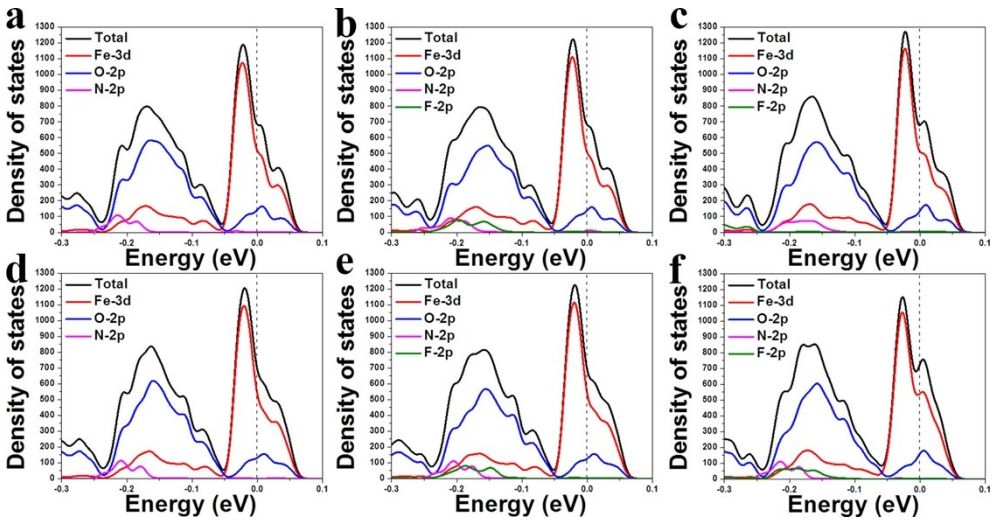

Fig. S21. Density of states of the N_2 adsorption on (200) surface of (a) β-FeO(OH-1), (b) β-FeO(OH,sF-1), (c) β-FeO(OH,iF-1), (d) β-FeO(OH-2), (e) β-FeO(OH,sF-2), and (f) β-FeO(OH,iF-2) for end-on configurations. The vertical dashed lines denote the Fermi energy.

Table S1. Comparison of electrocatalytic N_2 reduction performance of β-FeO(OH,F) with all Fe-based oxides and other transition metal oxides under ambient reaction conditions in aqueous media.

Catalyst	Electrolyte	NH_3 yield	FE(%)	Ref.
β-FeO(OH,F)	0.5 M $LiClO_4$	42.38 μg h^{-1} $mg^{-1}_{cat.}$	9.02	This work
Fe_2O_3-CNT	$KHCO_3$	0.22 μg h^{-1} cm^{-2}	0.15	7
30%Fe_2O_3-CNT	0.5 M KOH	0.52 μg·h^{-1}·cm^{-2}	0.164	8
Fe_2O_3 nanorod	0.1 M Na_2SO_4	15.9 μg h^{-1} $mg^{-1}_{cat.}$	0.94	9
γ-Fe_2O_3	0.1 M KOH	0.212 μg h^{-1} $mg^{-1}_{cat.}$	1.9	10
Fe_3O_4/Ti	0.1 M Na_2SO_4	3.63 μg h^{-1} cm^{-2}	2.6	11
o-Fe_2O_3-air	0.1 M KOH	0.46 μg·h^{-1}·cm^{-2}	6.04	12
β-FeOOH	0.5 M $LiClO_4$	23.32 μg h^{-1} $mg^{-1}_{cat.}$	6.7	13
Fe/Fe_3O_4	0.1 M PBS	0.19 μg h^{-1} cm^{-2}	8.29	14
MoO_3	0.1 M HCl	29.43 μg h^{-1} $mg^{-1}_{cat.}$	1.9	15
TiO_2	0.1 M Na_2SO_4	0.56 μg·h^{-1}·cm^{-2}	2.5	16
Mn_3O_4	0.1 M Na_2SO_4	11.6 μg h^{-1} $mg^{-1}_{cat.}$	3.0	17
VO_2 hollow microsphere	0.1 M Na_2SO_4	14.85 μg h^{-1} $mg^{-1}_{cat.}$	3.97	18
hollow Cr_2O_3	0.1 M Na_2SO_4	25.3 μg h^{-1} $mg^{-1}_{cat.}$	6.78	19
$Bi_4V_2O_{11}$/CeO_2	0.1 M HCl	23.21 mg h^{-1} $mg^{-1}_{cat.}$	10.16	20

References

1 D. Zhu, L. Zhang, R. E. Ruther and R. J. Hamers, *Nat. Mater.*, 2013, **12**, 836–841.

2 G. W. Watt and J. D. Chrisp, *Anal. Chem.*, 1952, **24**, 2006–2008.

3 B. Delley, *J. Chem. Phys.*, 1990, **92**, 508–517.

4 J. P. Perdew, K. Burke and M. Ernzerhof, *Phys. Rev. Lett.*, 1996, **77**, 3865.

5 B. Delley, *J. Chem. Phys.*, 2000, **113**, 7756–7764.

6 N. Govind, M. Petersen, G. Fitzgerald, D. King-Smith and J. Andzelm, *Comp. Mater. Sci.*, 2003, **28**, 250–258.

7 S. Chen, S. Perathoner, C. Ampelli, C. Mebrahtu, D. Su and G. Centi, *Angew. Chem.*, *Int. Ed.*, 2017, **56**, 2699–2703.

8 S. Chen, S. Perathoner, C. Ampelli, C. Mebrahtu, D. Su and G. Centi, *ACS Sustainable Chem. Eng*., 2017, **5**, 7393–7400.

9 X. Xiang, Z. Wang, X. Shi, M. Fan and X. Sun, *ChemCatChem.*, 2018, **10**, 4530–4535.

10 J. Kong, A. Lim, C. Yoon, J. H. Jang, H. C. Ham, J. Han, S. Nam, D. Kim, Y. E. Sung, J. Choi and H. S. Park, *ACS Sustainable Chem. Eng.*, 2017, **5**, 10986–10995.

11 Q. Liu, X. Zhang, B. Zhang, Y. Luo, G. Cui, F. Xie and X. Sun, *Nanoscale*, 2018, **10**, 14386–14389.

12 X. Cui, C. Tang, X. Liu, C. Wang, W. Ma and Q. Zhang, *Chem. Eur. J.*, 2018, **24**, 18494–18501.

13 X. Zhu, Z. Liu, Q. Liu, Y. Luo, X. Shi, A. M. Asiri, Y. Wu and X. Sun, *Chem. Commun.*, 2018, **54**, 11332–11335.

14 L. Hu, A. Khaniya, J. Wang, G. Chen, W. E. Kaden and X. Feng, *ACS Catal*., 2018, **8**, 9312–9319.

15 J. Han, X. Ji, X. Ren, G. Cui, L. Li, F. Xie, H. Wang, B. Li and X. Sun, *J. Mater. Chem. A*, 2018, **6**, 12974–12977.

16 R. Zhang, X. Ren, X. Shi, F. Xie, B. Zheng, X. Guo and X. Sun, *ACS Appl. Mater. Interfaces*, 2018, **10**, 28251–28255.

17 X. Wu, L. Xia, Y. Wang, W. Lu, Q. Liu, X. Shi and X. Sun, *Small*, 2018, **14**, 1803111.

18 R. Zhang, H. Guo, L. Yang, Y. Wang, Z. Niu, H. Huang, H. Chen, L. Xia, T. Li, X. Shi, X. Sun, B. Li and Q. Liu, *ChemElectroChem*, 2019, **6**, 1014–1018.

19 Y. Zhang, W. Qiu, Y. Ma, Y. Luo, Z. Tian, G. Cui, F. Xie, L. Chen, T. Li and X. Sun, *ACS Catal.*, 2018, **8**, 8540–8544.

20 C. Lv, C. Yan, G. Chen, Y. Ding, J. Sun, Y. Zhou and G. Yu, *Angew. Chem.*, *Int. Ed.***,** 2018, **130**, 6181–6184.